

Coulomb drag in anisotropic systems: a theoretical study on a double-layer phosphorene

S. Saberi-Pouya,¹ T. Vazifeshenas,^{1,*} M. Farmanbar,² and T. Salavati-fard³

¹*Department of Physics, Shahid Beheshti University, G. C., Evin, Tehran 1983969411, Iran*

²*Faculty of Science and Technology and MESA+ Institute for Nanotechnology, University of Twente, P.O. Box 217, 7500 AE Enschede, The Netherlands*

³*Department of Physics and Astronomy, University of Delaware, Newark, DE 19716, USA*

(Dated: December 3, 2024)

We theoretically study the Coulomb drag resistivity for a double-layer electron system with highly anisotropic parabolic band structure using Boltzmann transport theory. As an example, we choose a double-layer phosphorene, where we apply our formalism on and, in principle, can be tunable for other materials. Because of weakly bonding of two dimensional materials, rotation of one layer with respect to another layer plays an important role in anisotropic drag resistivity. In addition, the off-diagonal elements of drag resistivity tensor have non-zero values, at any temperature. We show that the anisotropic drag resistivity is very sensitive to the direction of momentum transfer between two layers due to highly anisotropic inter-layer electron-electron interaction and plasmon modes. In particular, the drag anisotropy ratio, ρ^{yy}/ρ^{xx} , varies from almost 2 to 3, by changing the temperature. Furthermore, we examine the dependence of drag resistivity and its anisotropy ratio on various parameters like inter-layer separation, electron density, short-range interaction and insulating substrate/spacer.

I. INTRODUCTION

The advent of two dimensional (2D) materials has sparked a considerable scientific interest due to their unique properties and their potential for applications in electronic devices. Atomically thin 2D materials, such as graphene,¹ monolayer black phosphorous (phosphorene),² hexagonal boron-nitride,³ and the transition-metal dichalcogenides (TMDs)⁴ represent a particularly interesting class of 2D materials including both semiconductors and metals. Phosphorene which is an interesting monatomic layered crystalline material, can be mechanically exfoliated from the bulk black phosphorus because of weak van der Waals interaction between layers.⁵ Unlike in group IV elemental materials, such as graphene,⁶ silicene⁶, or germanene,^{7,8} phosphorene is a semiconductor with puckered orthorhombic structure. This semiconductor has a nearly direct bandgap and its band structure shows a large anisotropy and high sensitivity to deformation.⁹ It suggests that crystallographic properties play an important role in the electronic behavior of this system. Recent studies reveal a high degree of anisotropic electronic and optical properties for the phosphorene, which implies the importance of this new 2D semiconductor as a promising candidate for electronic,^{10,11} thermoelectric,¹² and plasmonic applications.¹³⁻¹⁷

Double-layered 2D structures consisting of two parallel electron or hole systems which are kept in a close vicinity demand special attention due to many-body and transport properties.¹⁸⁻²¹ The inter-layer Coulomb interaction plays a significant role in these correlated systems. In Coulomb drag phenomenon, which is one of the interesting effects in a double-layer system, momentum can be transferred from interacting electrons in one layer to electrons in the adjacent layer.²² The momentum trans-

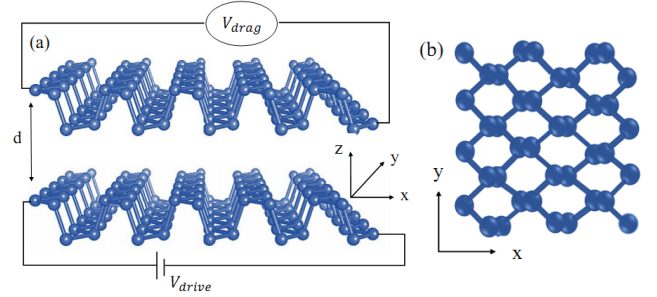


FIG. 1. (Color online)(a) Side view of a double-layer phosphorene system with the separation of d in the drag setup. (b) Top view of phosphorene.

fer takes place through inter-layer Coulomb interaction and without any carrier exchanges. This phenomenon has been previously studied in a few nanostructures such as double quantum wells (DQW).²³⁻²⁶

Owing to van der Waals bonding of 2D materials, one could spatially separate two layers of same kind experimentally by inserting a few layers of 2D insulator, for instance h -BN, to kill off any tunneling or hybridization between two layers. As it is shown by Gorbachev,²⁷ *et.al.*, a double-layer graphene system has a strong Coulomb drag resistivity.^{19,27-29} Phosphorene is a 2D semiconductor with the high anisotropy in its electronic structure, therefore, it becomes significantly important to investigate the effective mass anisotropy on the Coulomb drag.^{22,30-38}

In this paper, we investigate the effect of band anisotropy on the Coulomb drag resistivity in a double-layer electron system, consisting of two individual isolated layers which are coupled together via Coulomb interaction. We start from the expression for drag resis-

tivity based upon the semiclassical Boltzmann transport equation theory in the relaxation time approximation and develop a general formalism, which includes the effect of anisotropic energy dispersion and rotationally misaligned 2D systems. As an example, we apply this formalism to calculate Coulomb drag resistivity in a double-layer phosphorene system, see Fig.1. Numerical results show a strong drag resistivity dependence on the band anisotropy. It indicates that the drag resistivity along bigger mass, i.e., m_y , has a larger value. Furthermore, we discuss how the drag resistivity and its anisotropy ratio depend on the carrier density, inter-layer separation, rotation of layers and the choice of insulating substrate/spacer. The drag resistivity enhances substantially in y direction by adding the Hubbard local field correction (LFC) into our formalism, which includes the short-range exchange effect between electrons within the layer.

The rest of paper is organized as follows. Section II A, describes the model, theoretical formalism, and the Coulomb drag resistivity in 2D anisotropic systems. In Sec. II B, the dynamically screened inter-layer potential and also temperature-dependent anisotropic polarization function are presented. Section II C contains results for a double-layer phosphorene and the summary and conclusions are presented in Sec. III.

II. COULOMB DRAG RESISTIVITY IN 2D ANISOTROPIC SYSTEMS

A. Model

We consider a system composed of two parallel spatially separated 2D electron gases with anisotropic parabolic-like band structures. In this system the carriers are coupled through Coulomb interaction and there is no tunneling between layers so the Fermi energies and chemical potentials can be considered independently. The inter-layer Coulomb interaction can cause momentum transfer from the electrons in drive layer, layer 1, to the carriers in drag layer, layer 2, and generates a potential difference across the layers. In Fig.1(a) we show a schematic of the drag setup with phosphorene layers as anisotropic 2D electron gases. Also, a top view of phosphorene monolayer can be seen in Fig.1(b).

The drag (inter-layer) resistivity (ρ) can be defined as:³⁹

$$\sum_{\alpha=x,y} \rho_{21}^{\alpha\beta} J_{1,\alpha} = E_{2,\beta}, \quad (1)$$

where J and E are current density and electric field, respectively, the α and β indices label x and y components and $\rho_{21}^{\alpha\beta} = \rho_{12}^{\beta\alpha}$. The drag resistivity in linear regime has been calculated in a variety of theoretical approaches assuming energy-independent intra-layer momentum relaxation time and parabolic band structure. Using different theoretical approaches such as the memory function

formalism,³⁵ Kubo formula based on the leading-order diagrammatic perturbation theory⁴⁰ and the linear response Boltzmann transport equation. The drag resistivity matrix can be derived as:³⁹

$$\rho_{21}^{\alpha\beta} = \frac{\hbar}{2\pi e^2 n_1 n_2 K_B T} \int \frac{d^2 q}{(2\pi)^2} q_\alpha q_\beta \int_0^\infty d\omega \frac{|U_{21}(\mathbf{q}, \omega)|^2 \Im \Pi_2^\alpha(\mathbf{q}, \omega) \Im \Pi_1^\beta(\mathbf{q}, \omega)}{\sinh^2(\hbar\omega/2K_B T)} \quad (2)$$

where $U_{21}(\mathbf{q}, \omega)$ is the temperature-dependent dynamically screened inter-layer interaction and $\Pi_i(\mathbf{q}, \omega)$ being the 2D non-interacting polarization function of i th layer. In Sec. II C, we will rewrite eq.(2) to make it more convenient to use in a double-layer electron gas system with anisotropic band structure.

B. Inter-layer potential and temperature-dependent anisotropic polarization function

The dynamically screened inter-layer potential can be obtained by solving the corresponding Dyson equation:⁴¹

$$U_{ij}(\mathbf{q}, \omega) = \frac{V_{ij}(q)}{\det|\epsilon_{ij}(\mathbf{q}, \omega)|}, \quad (3)$$

where $V_{ij}(q) = \nu(q) \exp(-qd(1 - \delta_{ij}))$ is the unscreened 2D Coulomb interaction with d , is the layer spacing, $\nu(q) = 2\pi e^2/q\kappa$, κ being the average dielectric constant and $\epsilon_{ij}(\mathbf{q}, \omega)$, is the dynamic dielectric matrix of the system. For systems with high electron density it is reasonable to employ the RPA to calculate $\epsilon_{ij}(\mathbf{q}, \omega)$.^{42,43}

$$\epsilon_{ij}(\mathbf{q}, \omega) = \delta_{ij} + V_{ij}(q)\Pi_i(\mathbf{q}, \omega) \quad (4)$$

At low electron densities, the short-range local field effects are not negligible and must be included in dielectric matrix by replacing $(1 - G_{ij}(q))V_{ij}(q)$ for $V_{ij}(q)$ where $G_{ij}(q)$ denotes the static intra- ($i = j$) and inter-layer ($i \neq j$) elements of LFC matrix, respectively. Here we incorporate only the intra-layer components of LFC factor because of their stronger effect on the drag resistivity:⁴⁴

$$G_{ii}(q) = \frac{q}{2\sqrt{q^2 + k_F^2}}, \quad (5)$$

where $G(q)$ and $k_F = \sqrt{2\pi n}$ is the Hubbard LFC factor and the Fermi wave vector, respectively, with n being the electron density. For an electron gas system, the non-interacting polarization function can be obtained from the following equation:⁴⁵

$$\Pi_i(\mathbf{q}, \omega) = -\frac{g_s}{\nu} \sum_{\mathbf{k}} \frac{f(E_{\mathbf{q}}^i) - f(E_{\mathbf{k}+\mathbf{q}}^i)}{E_{\mathbf{q}}^i - E_{\mathbf{k}+\mathbf{q}}^i + \hbar\omega + i\eta} \quad (6)$$

Here $f(E_{\mathbf{q}}^i)$ is the Fermi distribution function in layer i at energy E corresponding to the wave vector \mathbf{q} , $g_s = 2$ is

spin degeneracy and η is the broadening parameter which accounts for disorder in the system. The temperature-dependent dynamic polarization function for intra-band transition in an anisotropic 2D material can be calculated by making use of the following anisotropic parabolic energy dispersion relation

$$E_{\mathbf{k}}^i = \frac{\hbar^2}{2} \left(\frac{k_x^2}{m_x} + \frac{k_y^2}{m_y} \right) - \mu_i, \quad (7)$$

in eq.(6) for the polarization function:

$$\begin{aligned} \frac{\Pi_i(\mathbf{q}, \omega)}{g_{2d}} = & - \int dK \frac{\Phi_i(K, T)}{Q} \left[\text{sgn}(\Re(Z_-)) \frac{1}{\sqrt{Z_-^2 - K^2}} \right. \\ & \left. - \text{sgn}(\Re(Z_+)) \frac{1}{\sqrt{Z_+^2 - K^2}} \right] \end{aligned} \quad (8)$$

In the above symmetric form of temperature-dependent anisotropic polarization function, we define $\mathbf{Q} = \sqrt{m_d/M}(\mathbf{q}/k_F)$, $\mathbf{K} = \sqrt{m_d/M}(\mathbf{k}/k_F)$ where M is the mass tensor with diagonal element m_x and m_y along x and y direction, and $m_d = \sqrt{m_x m_y}$ is the 2D density of state mass. Moreover, $g_{2d} = m_d/\pi\hbar^2$ and $Z_{\pm} = ((\hbar\omega + i\eta)/\hbar Q\nu_F) \pm (Q/2)$ with $\nu_F = \hbar k_F/m_d$ and $\Phi_i(K, T)$ is given by:

$$\Phi_i(K, T) = \frac{K}{1 + \exp[(K^2 E_F^i - \mu_i)/K_B T]} \quad (9)$$

where μ_i is the chemical potential of layer i , which is determined by the particle number conservation condition:⁴⁶

$$\mu_i + K_B T \ln[1 + \exp(-\mu_i/K_B T)] = E_F^i \quad (10)$$

Here, we consider $\mathbf{q} = q(\cos(\theta), \sin(\theta))$, in accordance to the notation in Ref. 13, to introduce rotational parameter for the layers. Rotational angel, τ_i , is defined as the angle between x -axis in the laboratory frame and x direction of the i th layer. So, we can write $Q = q\sqrt{m_d R_i}/k_F$ in which the orientation factor, R_i , is expressed as:

$$R_i = \left(\frac{\cos^2(\theta - \tau_i)}{m_x} + \frac{\sin^2(\theta - \tau_i)}{m_y} \right) \quad (11)$$

In case of double-layer phosphorene, we have $m_x \approx 0.15m_0$ and $m_y \approx 0.7m_0$ where m_0 is the free electron mass.⁴⁷ As it is well known, electronic collective modes of a double-layer system are obtained from zeros of the dielectric function determinant, Eq.(4), and in the presence of intra-band single particle excitations, there are two plasmon modes, the so-called acoustic and optical modes, showing linear $\omega_{ac}(q) \sim \sqrt{(R_1 R_2)/(R_1 + R_2)}q$ and square-root $\omega_{op} \sim \sqrt{(R_1 + R_2)}q$ behavior at small wave vectors, respectively, and dependence on the orientation factors.⁴⁷ To make the above discussion clearer,

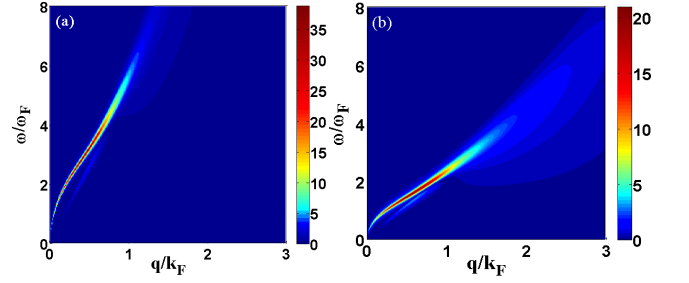


FIG. 2. (Color online) Loss function, $|\Im(1/dete(\mathbf{q}, \omega, T))|$, for two crystallographic directions (a) $\theta = 0$ and (b) $\theta = \pi/2$ at $T=100$ K with $d=5$ nm, $n = 3 \times 10^{12} \text{cm}^{-2}$ and $\eta=1$ meV.

we show the loss function of a system comprising of two parallel monolayer phosphorene separated by $d = 5$ nm at $T=100$ K for two main crystallographic directions: $\theta = 0$ and $\theta = \pi/2$, in Fig.2, respectively.

As we mentioned earlier, the RPA is reliable for systems with high electron densities. The density parameter $r_s = \sqrt{2}/(k_F a_B^*)$ with effective Bohr radius $a_B^* = \kappa/(e^2 m_d)$, which is defined as the average distance between electrons in a non-interacting 2D electron gas, gives a measure for reliability of the RPA. In this figure, we consider the same electron density in layers, $n_1 = n_2 = 3 \times 10^{12} \text{cm}^{-2}$, the substrate and spacer to be Al_2O_3 with $\kappa \approx 12$ that leads to an $r_s \approx 1.7$ for which employing the RPA is acceptable. One can recognize the lower-energy acoustic plasmon and higher-energy optical plasmon modes following different asymptotic behavior at small wave vectors in both panels of Fig.(2). Due to the anisotropic band structure, the long-lived plasmon modes disperse differently in such a way that the larger effective mass along y leads to smaller resonance frequencies.^{13,47,48}

It is worth pointing out that considering a very thin double-layer phosphorene system when, at the same time, we assume there is no tunneling between the two layers, is not actually a problematic consideration because the space between layers is filled by a slim dielectric material. Al_2O_3 and $h\text{-BN}$ have been successfully used as a substrate and spacer to make such thin heterostructures with no inter-layer tunneling.⁴⁹⁻⁵² Throughout this paper, we assume the substrate is a thick layer of the same material as spacer.

C. Drag effect in a double-layer phosphorene

In this section, we first derive a formula for the drag resistivity of a 2D anisotropic double-layer system with parabolic band structure and then solve it by making use of numerical methods. Eq.(2) is the general formula for drag resistivity based on the linearized Boltzmann transport equation. In the case of two coupled anisotropic layers, the off-diagonal components of drag resistivity tensor

have non-zero values unlike the isotropic systems such as double-layer graphene and two dimensional electron gas (2DEG). To make the difference more explicit, we rewrite

Eq.(2) as follows:

$$\rho_D^{\alpha\beta} = \frac{\hbar^2}{(2\pi)^3 e^2 n_1 n_2 K_B T} \int dq \int_0^\infty d\omega F^{\alpha\beta}(\mathbf{q}, \omega, T) \quad (12)$$

where $\rho_D^{\alpha\beta} = \rho_{21}^{\alpha\beta}$ and $F^{\alpha\beta}(\mathbf{q}, \omega, T)$ is defined as:

$$F^{\alpha\beta}(\mathbf{q}, \omega, T) = \int_0^{2\pi} d\theta \psi^{\alpha\beta}(\theta, \tau_1, \tau_2) \frac{q^3}{\sinh^2(\hbar\omega/2K_B T)} |U_{12}(q, \omega, T; \theta, \tau_1, \tau_2)|^2 \Im\Pi_1(q, \omega, T; \theta, \tau_1) \Im\Pi_2(q, \omega, T; \theta, \tau_2) \quad (13)$$

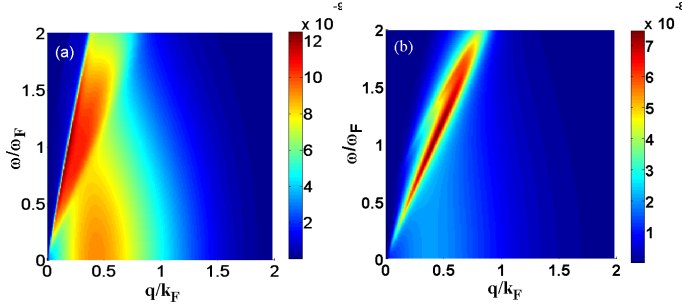


FIG. 3. (Color online) (a) $F^{xx}(q, \omega, T)$ and (b) $F^{yy}(q, \omega, T)$ for two aligned phosphorene monolayers sandwiched by Al_2O_3 layers at $T=100$ K with $d=5$ nm, $n=3 \times 10^{12} \text{cm}^{-2}$ and $\eta=1$ meV .

with $\psi^{\alpha\beta}$ given by

$$\psi^{\alpha\beta}(\theta, \tau_1, \tau_2) = \begin{cases} \cos(\theta - \tau_1) \cos(\theta - \tau_2), & \alpha = \beta = x \\ \sin(\theta - \tau_1) \sin(\theta - \tau_2), & \alpha = \beta = y \\ \cos(\theta - \tau_1) \sin(\theta - \tau_2), & \alpha = x, \beta = y \end{cases} \quad (14)$$

In order to understand how anisotropy affects the drag resistivity, it is worth looking into the integrand of Eq.(12), $F^{\alpha\beta}(\mathbf{q}, \omega, T)$, in more depth. In Fig.(3), we show $F^{\alpha\beta}(\mathbf{q}, \omega, T)$ for a coupled system composed of two aligned phosphorene monolayers separated by 5nm at $T=100$ K. Panel (a) and (b) demonstrate calculations for $\theta=0$ and $\theta=\pi/2$, respectively. We use the dimensionless variables q/k_F and ω/ω_F where $\omega_F = \hbar^{-1}E_F$. Note that the integrand has significant weight in $0 < q < k_F$ interval like in the case of conventional 2DEG⁴⁰ but its values are larger along the y direction. This is due to the greater effective mass of electrons in y direction which results in lower energies of the collective modes, and so enhances the plasmons contributions.^{30,40} Angular orientation of \mathbf{q} impacts the drag resistivity behavior considerably. We depict the integrand of Eq.(13) along x ($\alpha = \beta = x$) Fig.4(a) and y ($\alpha = \beta = y$) Fig.4(b) directions in an aligned layers system. At intermediate temperature $T \sim 100$ K, both modes (acoustic and optical) take part and single particle excitation spectrum

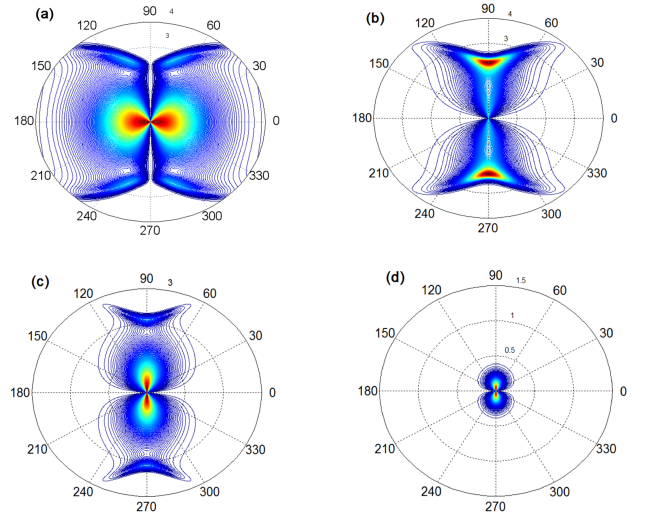


FIG. 4. (Color online) The integrand of Eq.(13) at $q = k_F$ for two aligned monolayers sandwiched by Al_2O_3 layers with $n=3 \times 10^{12} \text{cm}^{-2}$, and $\eta=1$ meV, $d=5$ nm, along (a) x and (b) y directions at $T=100$ K and along y direction at (c) $T=50$ K and (d) $T=10$ K. The radial and azimuthal coordinates denote ω/ω_F and the angular orientation of q , respectively.

is sufficiently broadened to contribute effectively. As it can be observed, the larger magnitude of integrand occurs around $\theta=0$ and 180° along the x direction and around $\theta=90^\circ$ and 270° for y direction, respectively. The integrand of Eq.(13) along the y direction is plotted in Fig.4(c) and (d) for two different temperatures: (c) $T=50$ K and (d) $T=10$ K. According to this figure, at $T=10$ K, the drag resistivity is mainly influenced by the acoustic mode which is lower in energy ($\omega < 0.5\omega_F$) and the optical mode contribution starts to appear at 50 K. Here, the radial and azimuthal coordinates denote ω/ω_F and the angular orientation of \mathbf{q} , respectively. First set of calculations of the drag resistivity in a double-layer phosphorene is presented in Fig.5. Here, we show the diagonal and off-diagonal elements of drag resistivity tensor calculated within the RPA versus temperature for two parallel aligned phosphorene monolayers which are sandwiched by Al_2O_3 layers and separated by a distance

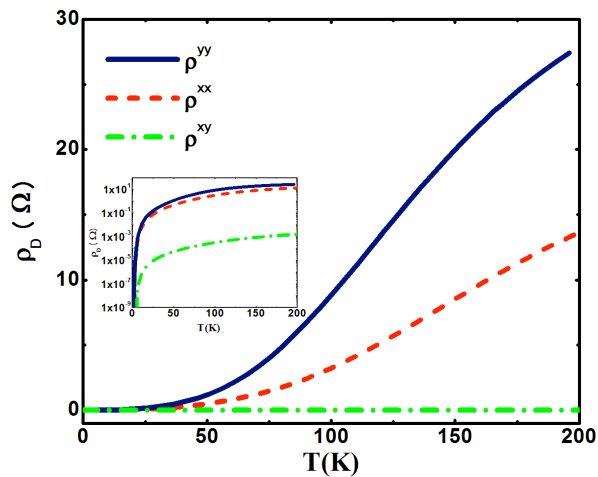


FIG. 5. (Color online) Anisotropic drag resistivity components, $\rho_D^{\alpha\beta}$ calculated within RPA as a function of temperature for two aligned phosphorene monolayers sandwiched by Al_2O_3 layers with $n = 3 \times 10^{12} \text{cm}^{-2}$ at $\eta = 1$ meV and $d = 5$ nm. The inset graph shows the same calculations in a logarithmic scale

of $d = 5$ nm. While the diagonal drag resistivity matrix elements increase similarly with temperature, there are significant differences between the values. Drag resistivity along the x direction, ρ^{xx} , is smaller than the drag resistivity along the y direction, ρ^{yy} , at any temperatures of interest with a drag anisotropy ratio, ρ^{yy}/ρ^{xx} , which approximately changes from 2 up to about 3. We believe a higher-energy resonance along x direction resulted from the smaller effective mass, as discussed before, accounts for this observation. Furthermore, our calculations show that the anisotropic effects can cause an interesting nonzero transversal drag resistivity, ρ^{xy} , which has not been seen previously in isotropic materials at zero magnetic field. While the transversal drag resistivity is smaller than the drag resistivity along x or y directions by a couple of orders of magnitude (see inset graph in Fig. 5), still, it should be measurable in an experiment. This effect, however, may exist in a double-layer structures which is subject to a perpendicularly applied magnetic field.^{27,37}

In order to understand how rotation of one layer with respect to the other, about the normal direction to the layers (z direction), impacts the behavior of drag resistivity, we present the calculations of the diagonal elements of the drag resistivity matrix for a couple of rotational angles in Fig. 6. Here, we set $\tau_1 = 0$ and $\tau_2 = \tau$. It is seen that as the angle of rotation increases, both diagonal elements of drag resistivity decrease, considerably. This observation can be understood through this fact that by increasing the angle of rotation one of the plasmonic branches gets forced into the damped regime. As a result, the contribution of plasmons to the Coulomb drag phenomenon, which is known to be significant, decreases.

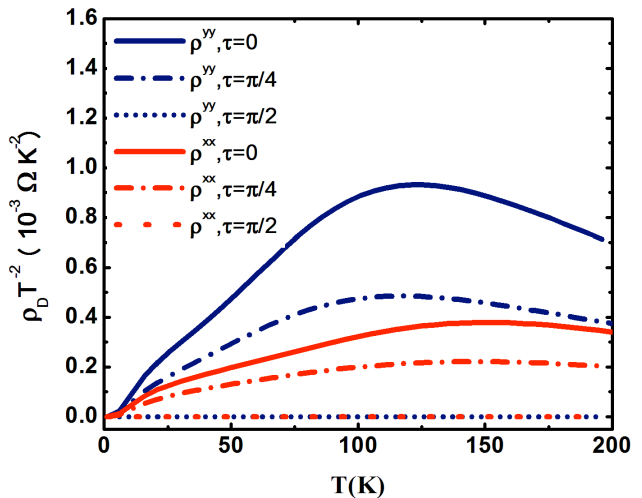


FIG. 6. (Color online) Scaled drag resistivity $\rho_D T^{-2}$ as a function of temperature for different angles with $n = 3 \times 10^{12} \text{cm}^{-2}$, and $\eta = 1$ meV, $d = 5$ nm. The phosphorene layers are sandwiched by Al_2O_3 layers.

Another interesting geometrical effect in a double-layer phosphorene structure comes from changing the inter-layer distance which is presented in Fig. 7. Fig. 7(a) is a 3D plot showing the variation of $\rho^{yy} T^{-2}$ as a function of layer spacing and temperature. It can be observed that the peaks occur at intermediate temperatures where the plasmon contribution to the drag resistivity is significant, over the whole range of inter-layer distances. Also, the scaled drag resistivity decreases strongly by increasing the separation between two layers at all temperatures. One can recognize the inter-layer interaction, which decays exponentially with the increasing distance between layers and decreases by acoustic modes shifting toward higher energies, are responsible for this behaviour. Having said that, it is worth pointing out that the changing inter-layer distance does not change the drag anisotropy ratio, significantly. To trace this behavior, we plot both scaled ρ^{xx} and ρ^{yy} as functions of temperature for two different layer spacings: $d = 2$ nm and 5 nm in Fig. 7(b), which shows the anisotropy ratio is less dependent on the inter-layer distance.

The effect of electron density on the drag transresistivity is also of interest, so we illustrate it in Fig. 8(a). As expected for double-layers systems, with increase in electron density the Coulomb drag decreases and the resistivity peak moves toward higher temperature.³⁰ Moreover, it is worth mentioning that the anisotropic effect is more pronounced at lower electron density. By including the Hubbard zero-temperature LFC, improvement over the RPA results is studied in Fig. 8(b). Here, we employ the intra-layer local field factor, Eq. (5), which is responsible for most of the drag resistivity enhancement by the short-range interaction effects.⁵³ Exchange interaction which is taken into account by the Hubbard LFC impacts the inter-layer interaction through the dielectric

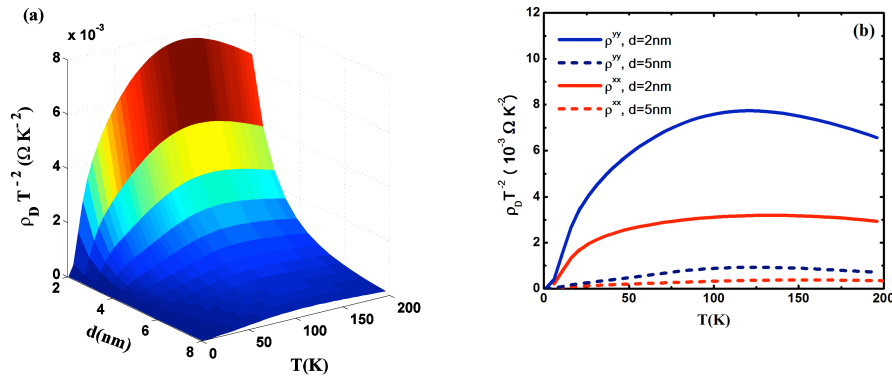


FIG. 7. (Color online) Scaled drag resistivity calculated within RPA (a) along y direction as a function of temperature and the distance between two layers and (b) along x and y directions as a function of temperature with two different inter-layer separations. Here, $n = 3 \times 10^{12} \text{cm}^{-2}$ and $\eta = 1 \text{ meV}$ and system comprising of two aligned phosphorene monolayers sandwiched by Al_2O_3 .

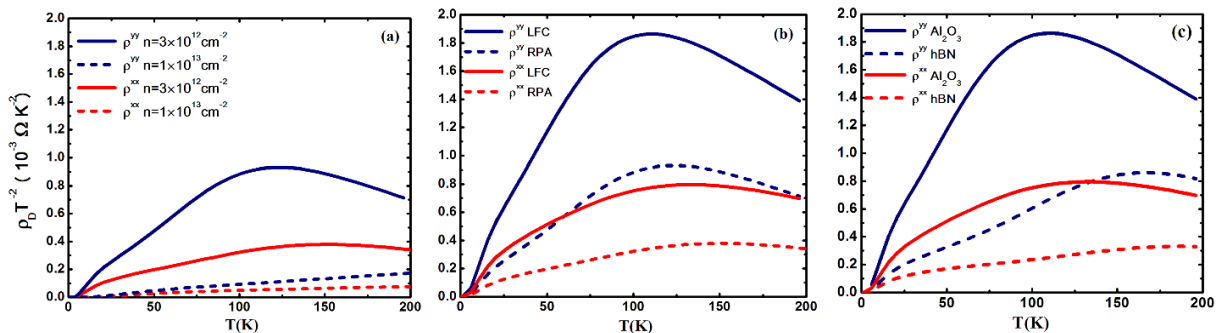


FIG. 8. (Color online) Scaled drag resistivity, $\rho_D T^{-2}$, as a function of temperature for two aligned phosphorene monolayers sandwiched by Al_2O_3 and calculated (a) within RPA at two different electron densities $n = 3 \times 10^{12} \text{cm}^{-2}$ (solid line) and $n = 1 \times 10^{13} \text{cm}^{-2}$ (dashed line) (b) within RPA and Hubbard local field approximation at electron density $n = 3 \times 10^{12} \text{cm}^{-2}$ and (c) sandwiched by Al_2O_3 and $h\text{-BN}$ calculated within Hubbard local field approximation at electron density $n = 3 \times 10^{12} \text{cm}^{-2}$. Here we set $d = 5 \text{ nm}$ and $\eta = 1 \text{ meV}$.

function of the system (see Eq.(3)). Our calculations show that including the LFC factor enhances the drag resistivity results notably by strengthening the inter-layer interaction.⁵³ Furthermore, for the parameter used here one can obtain the anisotropy ratio values is almost the same for both approximations.

Finally, we investigate the effects of substrate and spacer dielectric materials on anisotropic drag resistivity by considering two already experimentally used insulators, namely Al_2O_3 ⁵² and $h\text{-BN}$,⁵⁰ in phosphorene systems. Here, we assume $n = 3 \times 10^{12} \text{cm}^{-2}$ corresponding in $h\text{-BN}$ case to density parameter $r_s \sim 5$ which makes it necessary to consider the LFC factor in our calculation. Results indicate that the anisotropic drag resistivity has higher values, at any temperatures, when Al_2O_3 is used as spacer/substrate compared with the case in which $h\text{-BN}$ is used (see Fig.8) due to a larger dielectric constant of Al_2O_3 . Employing the high- κ materials as substrates/spacers reduces screening and as a

result, enhances the inter-layer electron-electron interactions. From this figure, it can be observed that the change of insulating materials have negligible effect on drag anisotropy ratio.

III. CONCLUSION

To summarize, we have derived a formula for the anisotropic drag resistivity in a structure composed of two spatially separated two dimensional electron gas systems with parabolic band structures. We have assumed the electron gases are sandwiched by insulators so that there is no tunneling between the layers. We have considered double-layer phosphorene to apply our anisotropic drag theory on. Our numerical results have confirmed that the drag resistivity depends not only upon the usually-considered parameters such as temperature, inter-layer separation, carrier density and nature of ele-

mentary excitations, but also on direction of the transferred momentum between the two layers as well as the rotational parameter. The calculations have also shown that while the diagonal elements of anisotropic drag resistivity tensor have different values due to different electron effective masses along x and y directions, at any temperatures of interest, there are non-zero off-diagonal elements. The non-zero off-diagonal elements have not been reported before in a two dimensional coupled system without an applied magnetic field. According to the numerical results, both diagonal elements of anisotropic drag resistivity tensor increase with decreasing inter-layer separation and electron density. We obtain that, the anisotropic ratio varies with the change of temperature and electronic density, effectively. To improve RPA results at low electron density, we have included the zero temperature Hubbard LFC factor in calculations and

shown that LFC changes the results strongly. Moreover, the effects of substrate/spacer on the anisotropic drag resistivity have been studied in this work. We have shown that a substrate/spacers with high dielectric constant, is able to increase anisotropic drag resistivity considerably.

These results provide qualitative insight into the impact that anisotropic band structure can have on drag resistivity, as an important transport quantity, in a coupled 2D structure. The present work also suggests that the rotational parameter of layers can be considered as an extra degree of freedom for the applications of momentum transfer between coupled layers.

ACKNOWLEDGMENTS

The authors declare no competing financial interest.

-
- * t-vazifeh@sbu.ac.ir
- ¹ A. K. Geim and I. V. Grigorieva, *Nature* **499**, 419 (2013).
 - ² X. Ling, H. Wang, S. Huang, F. Xia, and M. S. Dresselhaus, *Proc. Natl. Acad. Sci. U.S.A.* **112**, 4523 (2015).
 - ³ M. Xu, T. Liang, M. Shi, and H. Chen, *Chem. Rev.* **113**, 3766 (2013).
 - ⁴ G.-B. Liu, D. Xiao, Y. Yao, X. Xu, and W. Yao, *Chem. Soc. Rev.* **44**, 2643 (2015).
 - ⁵ L. Li, Y. Yu, G. J. Ye, Q. Ge, X. Ou, H. Wu, D. Feng, X. H. Chen, and Y. Zhang, *Nat. Nanotechnol.* **9**, 372 (2014).
 - ⁶ P. Vogt, P. De Padova, C. Quaresima, J. Avila, E. Frantzeskakis, M. C. Asensio, A. Resta, B. Ealet, and G. Le Lay, *Phys. Rev. Lett.* **108**, 155501 (2012).
 - ⁷ A. Acun, L. Zhang, P. Bampoulis, M. Farmanbar, A. van Houselt, A. N. Rudenko, M. Lingenfelder, G. Brocks, B. Poelsema, M. I. Katsnelson, and H. J. W. Zandvliet, *J. Phys.: Condens. Matter.* **27**, 443002 (2015).
 - ⁸ S. Cahangirov, M. Topsakal, E. Aktürk, H. Şahin, and S. Ciraci, *Phys. Rev. Lett.* **102**, 236804 (2009).
 - ⁹ A. S. Rodin, A. Carvalho, and A. H. Castro Neto, *Phys. Rev. Lett.* **112**, 176801 (2014).
 - ¹⁰ H. Liu, A. T. Neal, Z. Zhu, Z. Luo, X. Xu, D. Tománek, and P. D. Ye, *ACS nano* **8**, 4033 (2014).
 - ¹¹ B. Sa, Y.-L. Li, Z. Sun, J. Qi, C. Wen, and B. Wu, *Nanotechnology* **26**, 215205 (2015).
 - ¹² T.-H. Liu and C.-C. Chang, *Nanoscale* **7**, 4598 (2015).
 - ¹³ T. Low, R. Roldán, H. Wang, F. Xia, P. Avouris, L. M. Moreno, and F. Guinea, *Phys. Rev. Lett.* **113**, 106802 (2014).
 - ¹⁴ F. Xia, H. Wang, and Y. Jia, *Nat. Commun.* **5**, 4458 (2014).
 - ¹⁵ M. Engel, M. Steiner, and P. Avouris, *Nano Lett.* **14**, 6414 (2014).
 - ¹⁶ A. N. Rudenko and M. I. Katsnelson, *Phys. Rev. B* **89**, 201408 (2014).
 - ¹⁷ T. Low, A. S. Rodin, A. Carvalho, Y. Jiang, H. Wang, F. Xia, and A. H. Castro Neto, *Phys. Rev. B* **90**, 075434 (2014).
 - ¹⁸ L. Shulenburger, A. Baczewski, Z. Zhu, J. Guan, and D. Tománek, *Nano Lett.* **15**, 8170 (2015).
 - ¹⁹ T. Vazifeshenas, T. Amlaki, M. Farmanbar, and F. Parhizgar, *Phys. Lett. A* **374**, 4899 (2010).
 - ²⁰ G. R. Berdiyrov, H. Bahlouli, and F. M. Peeters, *J. Appl. Phys.* **117**, 225101 (2015).
 - ²¹ R. Roldán and L. Brey, *Phys. Rev. B* **88**, 115420 (2013).
 - ²² B. Narozhny and A. Levchenko, *arXiv:1505.07468* (2015).
 - ²³ A. Yurtsever, V. Moldoveanu, and B. Tanatar, *Solid State Commun.* **125**, 575 (2003).
 - ²⁴ B. Tanatar and A. K. Das, *Phys. Rev. B* **61**, 15959 (2000).
 - ²⁵ T. Vazifeshenas and A. Eskourchi, *Physica E* **36**, 147 (2007).
 - ²⁶ T. Vazifeshenas and T. Salavati-fard, *Physica B* **462**, 112 (2015).
 - ²⁷ R. V. Gorbachev, A. K. Geim, M. I. Katsnelson, K. S. Novoselov, T. Tudorovskiy, I. V. Grigorieva, A. H. MacDonald, S. V. Morozov, K. Watanabe, T. Taniguchi, and L. A. Ponomarenko, *Nature Physics* **8**, 896 (2012).
 - ²⁸ W.-K. Tse, B. Y.-K. Hu, and S. Das Sarma, *Phys. Rev. B* **76**, 081401 (2007).
 - ²⁹ E. H. Hwang, R. Sensarma, and S. Das Sarma, *Phys. Rev. B* **84**, 245441 (2011).
 - ³⁰ K. Flensberg and B. Y.-K. Hu, *Phys. Rev. Lett.* **73**, 3572 (1994).
 - ³¹ P. M. Solomon, P. J. Price, D. J. Frank, and D. C. La Tulipe, *Phys. Rev. Lett.* **63**, 2508 (1989).
 - ³² H. Noh, S. Zelakiewicz, X. G. Feng, T. J. Gramila, L. N. Pfeiffer, and K. W. West, *Phys. Rev. B* **58**, 12621 (1998).
 - ³³ H. C. Tso, P. Vasilopoulos, and F. M. Peeters, *Phys. Rev. Lett.* **68**, 2516 (1992).
 - ³⁴ A.-P. Jauho and H. Smith, *Phys. Rev. B* **47**, 4420 (1993).
 - ³⁵ L. Zheng and A. H. MacDonald, *Phys. Rev. B* **48**, 8203 (1993).
 - ³⁶ C. P. Weber, N. Gedik, J. E. Moore, J. Orenstein, J. Stephens, and D. D. Awschalom, *Nature* **437**, 1330 (2005).
 - ³⁷ T. J. Gramila, J. P. Eisenstein, A. H. MacDonald, L. N. Pfeiffer, and K. W. West, *Phys. Rev. Lett.* **66**, 1216 (1991).
 - ³⁸ A. F. Croxall, K. Das Gupta, C. A. Nicoll, M. Thangaraj, H. E. Beere, I. Farrer, D. A. Ritchie, and M. Pepper, *Phys. Rev. Lett.* **101**, 246801 (2008).

- ³⁹ K. Flensberg and B. Y.-K. Hu, *Phys. Rev. B* **52**, 14796 (1995).
- ⁴⁰ K. Flensberg, B. Y.-K. Hu, A.-P. Jauho, and J. M. Kinaret, *Phys. Rev. B* **52**, 14761 (1995).
- ⁴¹ S. M. Badalyan and F. M. Peeters, *Phys. Rev. B* **86**, 121405 (2012).
- ⁴² E. H. Hwang and S. Das Sarma, *Phys. Rev. B* **80**, 205405 (2009).
- ⁴³ W.-L. You and X.-F. Wang, *Nanotechnology* **23**, 505204 (2012).
- ⁴⁴ M. Jonson, *J. Phys. C: Sol. State Phys.* **9**, 3055 (1976).
- ⁴⁵ D. Bohm and D. Pines, *Phys. Rev.* **92**, 609 (1953).
- ⁴⁶ N. Ashcroft and N. Mermin, *Solid State Physics* (Saunders College, Philadelphia, 1976).
- ⁴⁷ A. S. Rodin and A. H. Castro Neto, *Phys. Rev. B* **91**, 075422 (2015).
- ⁴⁸ F. Jin, R. Roldán, M. I. Katsnelson, and S. Yuan, *Phys. Rev. B* **92**, 115440 (2015).
- ⁴⁹ J.-S. Kim, Y. Liu, W. Zhu, S. Kim, D. Wu, L. Tao, A. Dodabalapur, K. Lai, and D. Akinwande, *Sci. Rep.* **5**, 8989 (2015).
- ⁵⁰ X. Chen, Y. Wu, Z. Wu, Y. Han, S. Xu, L. Wang, W. Ye, T. Han, Y. He, Y. Cai, and N. Wang, *Nat. Commun.* **6**, 7315 (2015).
- ⁵¹ H. Zhu, S. McDonnell, X. Qin, A. Azcatl, L. Cheng, R. Addou, J. Kim, P. D. Ye, and R. M. Wallace, *ACS. Appl. Mater. Inter.* **7**, 13038 (2015).
- ⁵² X. Luo, Y. Rahbariagh, J. Hwang, H. Liu, Y. Du, and P. Ye, *Electron Device Letters, IEEE* **35**, 1314 (2014).
- ⁵³ L. Świerkowski, J. Szymański, and Z. W. Gortel, *Phys. Rev. Lett.* **74**, 3245 (1995).